

# Oxygen adsorption on Mo(112) surface studied by *ab initio* genetic algorithm and experiment

Marek Sierka,<sup>a)</sup> Tanya K. Todorova, and Joachim Sauer

*Institut für Chemie, Humboldt-Universität zu Berlin, Unter den Linden 6, 10099 Berlin, Germany*

Sarp Kaya, Dario Stacchiola, Jonas Weissenrieder,  
Shamil Shaikhutdinov, and Hans-Joachim Freund

*Fritz-Haber-Institut der Max-Planck-Gesellschaft, Faradayweg 4-6, 14195 Berlin, Germany*

(Received 3 November 2006; accepted 30 April 2007; published online 20 June 2007)

Density functional theory in combination with genetic algorithm is applied to determine the atomic models of  $p(1 \times 2)$  and  $p(1 \times 3)$  surface structures observed upon oxygen adsorption on a Mo(112) surface. The authors' simulations reveal an unusual flexibility of Mo(112) resulting in oxygen-induced reconstructions and lead to more stable structures than any suggested so far. Comparison of the stabilities of the predicted models shows that different  $p(1 \times 2)$  and  $p(1 \times 3)$  structures may coexist over a wide range of oxygen pressures. A pure  $p(1 \times 2)$  structure can be obtained only in a narrow region of oxygen pressures. In contrast, a pure  $p(1 \times 3)$  structure cannot exist as a stable phase. The results of simulations are fully supported by a multitude of experimental data obtained from low energy electron diffraction, x-ray photoelectron spectroscopy, and scanning tunneling microscopy. © 2007 American Institute of Physics. [DOI: 10.1063/1.2743427]

## I. INTRODUCTION

Molybdenum and molybdenum oxides attract substantial interest because of their important applications as industrial catalysts in selective oxidation of hydrocarbons and alcohols, hydrodesulfurization, and  $\text{NO}_x$  reduction.<sup>1</sup> Molybdenum based catalysts have shown great promise in the liquefaction of coal, which is regarded as their most important future catalytic usage. Molybdenum single crystals have been successfully used as a substrate for the preparation of ultrathin oxide films, e.g.,  $\text{SiO}_2$ ,<sup>2,3</sup>  $\text{Al}_2\text{O}_3$ ,<sup>4</sup>  $\text{TiO}_2$ ,<sup>5</sup> and  $\text{MgO}$ <sup>6</sup> with potential applications as insulating layers in microelectronic devices, protective films against corrosion, and as model supports in heterogeneous catalysis. The synthesis of such films usually starts with oxygen adsorption on a clean metal surface. Therefore, dissociation and adsorption of oxygen, oxygen-induced structure changes, and oxide formation on stable low-index molybdenum surfaces have been subject of a number of experimental and theoretical studies.<sup>7-12</sup>

The Mo(112) surface shows a ridge-and-through structure with the top layer Mo atoms forming close-packed rows along the  $[\bar{1}\bar{1}1]$  direction separated from each other by 4.45 Å in  $[\bar{1}\bar{1}0]$  direction. Depending on the experimental conditions various surface structures have been observed upon oxygen adsorption on Mo(112):  $p(3 \times 9)$ ,<sup>7</sup>  $p(6 \times 12)$ ,<sup>7</sup>  $p(1 \times 2)$ ,<sup>8,9</sup>  $p(1 \times 3)$ ,<sup>9</sup>  $p(2 \times 1)$ ,<sup>10</sup>  $c(4 \times 2)$ ,<sup>10</sup> and  $p(2 \times 3)$ .<sup>11</sup> The oxygen-induced  $p(1 \times 3)$  structure has been postulated as a precursor for the epitaxial formation of  $\text{MoO}_2(100)$ .<sup>9</sup> The detailed atomic structure of these surfaces is still under debate. Even for the simplest  $p(1 \times 2)$  one, several models have been proposed based either on experimental data<sup>8,9</sup> or

theoretical calculations,<sup>12</sup> involving both unreconstructed<sup>8,12</sup> and reconstructed<sup>9</sup> surfaces. Similarly, for  $p(1 \times 3)$ - and  $p(2 \times 3)$ -Mo(112) surface structures, oxygen-induced reconstructions have been postulated.<sup>9,11</sup>

Obviously, the problem in deriving reliable atomic structure models of observed surfaces from theoretical calculations arises from the large number of possible adsorption sites and surface configurations (reconstructed versus unreconstructed). Even the simplest  $p(1 \times 2)$  surface unit cell has 16 potential adsorption sites and may lead to a large number of possible structures. Their manual constructions followed by structure optimizations would be a formidable task. In many cases experimental data such as atomically resolved scanning tunneling microscopy (STM) images can provide some information about possible arrangement of atoms, but data interpretation relies to a large extent on intuition. Recently, several techniques for automatic determination of the most stable surface structures, such as genetic algorithm<sup>13,14</sup> (GA) and Monte Carlo<sup>15</sup> methods have been proposed. The GA approach appears particularly efficient. It requires only the periodic vectors of the surface unit cell and the chemical potentials of the constituent species as input. The number of atoms involved in the adsorption and reconstruction, as well as their most favorable bonding geometry under different conditions, is obtained automatically within the same GA search.

Here we present our own implementation of the GA following the original idea of Chuang *et al.*<sup>13</sup> and apply it to the  $p(1 \times 2)$  and  $p(1 \times 3)$  structures observed upon oxygen adsorption on the Mo(112) surface. We demonstrate that the most favorable atomic models found in our GA simulations are more stable than any other suggested so far. A comparison of the stability of the predicted models shows that different  $p(1 \times 2)$  and  $p(1 \times 3)$  structures coexist over a wide

<sup>a)</sup>Author to whom correspondence should be addressed. Electronic mail: marek.sierka@chemie.hu-berlin.de

range of oxygen pressures. They are characterized by a missing-row-type reconstructed Mo(112) surface forming different reconstruction patterns. Results of our calculations provide a straightforward explanation of experimental low energy electron diffraction (LEED), x-ray photoelectron spectroscopy (XPS), scanning tunneling microscopy, and high resolution electron energy loss spectroscopy (HREELS) data.

## II. COMPUTATIONAL DETAILS

### A. Methods

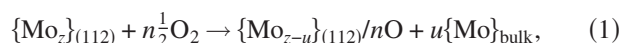
All calculations are based on density functional theory (DFT) and performed using the Vienna Ab initio Simulation Package<sup>16,17</sup> (VASP) along with the Perdew-Wang<sup>18</sup> (PW91) exchange-correlation functional. The electron-ion interactions were described by the projector augmented-wave (PAW) method<sup>19</sup> in the implementation of Kresse and Joubert.<sup>20</sup> We use a dual computational strategy. For the GA runs a plane-wave basis set with an energy cutoff of 200 eV along with appropriate PAW potentials and a  $(2 \times 2 \times 1)$  Monkhorst-Pack grid<sup>21</sup> for the integration of the Brillouin zone are used. The final structure optimizations and energy evaluations of the atomic structure models resulting from the GA runs apply an energy cutoff of 400 eV and a  $(12 \times 4 \times 1)$   $k$ -point grid. We note that the energies obtained with the first, lower accuracy setup exactly reproduce (with a deviation of less than 0.1 eV) the ordering of the structures obtained at the second, higher level. The STM images are simulated from the self-consistent charge density employing the Tersoff-Hamann approach.<sup>22</sup> Calculations of the vibrational spectra use a central finite difference method with intensities obtained from the derivatives of the dipole moment component perpendicular to the surface. To compensate for systematic errors of DFT the vibrational frequencies are scaled by an empirical factor<sup>23</sup> of 1.0382 derived from a comparison between experimental<sup>24</sup> and calculated frequencies for bulk MoO<sub>2</sub>.

### B. Substrate models

The surface unit cells are modeled using orthorhombic  $(1 \times 2)$  and  $(1 \times 3)$  supercells with the lattice constants  $a_0 = 2.73$ ,  $b_0 = 8.92$  Å and  $a_0 = 2.73$ ,  $b_0 = 13.39$  Å, respectively. In all structure optimizations the two bottom layers of the Mo(112) substrate are kept fixed at their bulk positions.

### C. Thermodynamic stability of the models

We denote structure models containing  $n$  oxygen atoms per surface unit cell of a given periodicity as Mo(112)/ $n$ O. To compare the stabilities of different models we use the formation energy  $\Delta E_{\text{form}}$  from a clean Mo(112) surface and molecular oxygen,



where  $u$  defines the number of Mo atoms removed to form a missing-row-type reconstructed surface. The total number of Mo atoms in a unit cell is  $z$ . Thus,  $\Delta E_{\text{form}}$  is defined as

$$\Delta E_{\text{form}} = E^{\{\text{Mo}_{z-u}\}_{(112)}/n\text{O}} + uE^{\{\text{Mo}\}_{\text{bulk}}} - E^{\{\text{Mo}_z\}_{(112)}} - n\frac{1}{2}E^{\text{O}_2}, \quad (2)$$

where  $E^{\{\text{Mo}_{z-u}\}_{(112)}/n\text{O}}$  corresponds to the energy of the given Mo(112)/ $n$ O model,  $E^{\{\text{Mo}_z\}_{(112)}}$ ,  $E^{\{\text{Mo}\}_{\text{bulk}}}$ , and  $E^{\text{O}_2}$  are the energies of the clean Mo(112) surface with  $z$  atoms in the unit cell, of bulk Mo, and of an oxygen molecule, respectively. Since the models differ not only by their atomic structure but also by their chemical composition, the values of  $\Delta E_{\text{form}}$  cannot be used directly to compare the stabilities. Instead, we consider the surface-related free energy change of reaction (1)  $\Delta\gamma$

$$\Delta\gamma(T, p) = \frac{1}{S}[\Delta E_{\text{form}} - n\Delta\mu_{\text{O}}(T, p)], \quad (3)$$

with  $\Delta\mu_{\text{O}}(T, p) = \mu_{\text{O}} - 1/2E^{\text{O}_2}$ , where  $\mu_{\text{O}}$  is the oxygen chemical potential and  $S$  is the surface area. The free energy is calculated neglecting zero-point vibrational energy, vibrational entropy, and vibrational enthalpy contributions. The oxygen chemical potential is related to oxygen partial pressure at a given temperature, assuming that the surface is in thermodynamic equilibrium with the gas phase O<sub>2</sub>.<sup>25</sup>

### D. Genetic algorithm

Following the idea of Chuang *et al.*<sup>13</sup> our implementation is based on the evolutionary approach in which different surface structures form a population. The algorithm starts with a population of  $M$  randomly generated structures. In the present case  $M=15-25$  initial models are obtained by a random distribution of oxygen atoms on a given Mo(112) surface. The number of oxygen atoms for each structure is chosen randomly between 1 and  $k$ . The algorithm is quite insensitive to the choice of  $k$  and we use  $k=3$  oxygen atoms per  $(1 \times 1)$  Mo(112) surface unit cell. The structures in the initial pool are optimized using a conjugate-gradient technique. The subsequent algorithm steps proceed as follows.

*Fitness evaluation.* The fitness  $f_i$  of each individual in the current population is evaluated. We use a fitness function based on the surface-related free energy change  $\Delta\gamma$  of reaction (1), Eq. (3)

$$f_i = \frac{\exp[-\Delta\gamma/\beta(\Delta\gamma_{\text{max}} - \Delta\gamma_{\text{min}})]}{\sum_i^M f_i}, \quad (4)$$

where  $\Delta\gamma_{\text{max}}$  and  $\Delta\gamma_{\text{min}}$  are the maximum and minimum values of  $\Delta\gamma$  in the population and  $\beta$  is an adjustable parameter ( $\beta=0.5$  in our calculations). This definition of  $f_i$  automatically increases the selection pressure with a decreasing range of  $\Delta\gamma$  in the population.

*Crossover.* The evolution from one generation to the next takes place by crossover. Two structures are selected from the population to be parents for crossover. We use a roulette wheel selection,<sup>26</sup> with selection probability proportional to the value of the fitness function. The crossover operation adapted in our implementation is similar to the one used by Chuang *et al.*<sup>13</sup> The topmost parts of the parent structures are sectioned by an arbitrary plane and then combined to create a child structure. To prevent creation of child

structures with too small interatomic distances at the junction between the two parent substructures, we discard atoms with unreasonably small interatomic distances. In each generation, a number of  $m$  ( $m=8-10$ ) crossover operations are performed. The resulting  $m$  children structures are then optimized.

**Mutation.** Mutation operations prevent premature convergence of the GA and provide additional structural diversity. Here the mutation is performed by removing or adding atoms at random positions of randomly chosen parent structures. Mutated structures are locally optimized and added to the population. The mutation rate is kept below 1% in all GA runs.

**Selection of the next generation.** The parent structures of the current generation, optimized children structures obtained by the crossover operations, and mutated structures form a new population. In order to maintain a maximum diversity during the GA runs we sort the population into groups of similar structures. This is achieved by comparing the number and positions of the atoms in the unit cell as well as the interatomic bond distances. Next, the structures are ordered in a list that includes the most stable structure (in terms of  $\Delta\gamma$ ) from each group, then the second most stable, and so on. The next generation of parent structures is created by choosing  $M$  topmost structures from the list.

### III. EXPERIMENTAL DETAILS

The experiments were carried out in ultrahigh vacuum (UHV) chamber (base pressure below  $1 \times 10^{-10}$  mbar), equipped with low energy electron diffraction (Omicron), XPS (Scienta SES-200), IR spectrometer (Bruker IFS 66v/s), STM (Omicron), and standard facilities for surface cleaning.<sup>11</sup> Sample heating was performed by electron bombardment from a thoriated tungsten filament placed close to the backside of the sample. The temperature was measured by a WRe 5%/WRe 26% thermocouple spot-welded to the edge of the Mo crystal. The Mo(112) (99.99%, Mateck) single crystal was cleaned via cycles of annealing in  $1 \times 10^{-6}$  mbar  $O_2$  at 800 K followed by a flash to 2300 K in UHV, until XPS and LEED measurements indicated a clean, well-ordered surface. Oxygen was dosed by backfilling the chamber. Exposures are given in langmuirs ( $1 \text{ L} = 1 \times 10^{-6}$  Torr s).

### IV. RESULTS AND DISCUSSION

Figure 1 shows possible oxygen adsorption sites on the Mo(112) surface. They are denoted as atop, short- and long-bridge, as well as pseudothreefold hollow sites. We use abbreviations  $p(1 \times 2)\text{-Mo}(112)/nO$  and  $p(1 \times 3)\text{-Mo}(112)/nO$  to distinguish models with  $n$  oxygen atoms adsorbed per surface unit cell of the given periodicity.

#### A. $p(1 \times 2)\text{-Mo}(112)/nO$ models

Figure 2 summarizes the  $p(1 \times 2)\text{-Mo}(112)/nO$  structure models obtained in our GA simulations. In models A–D the Mo surface is reconstructed; i.e., every third topmost Mo row along the  $[\bar{1}\bar{1}1]$  direction is missing and a different num-

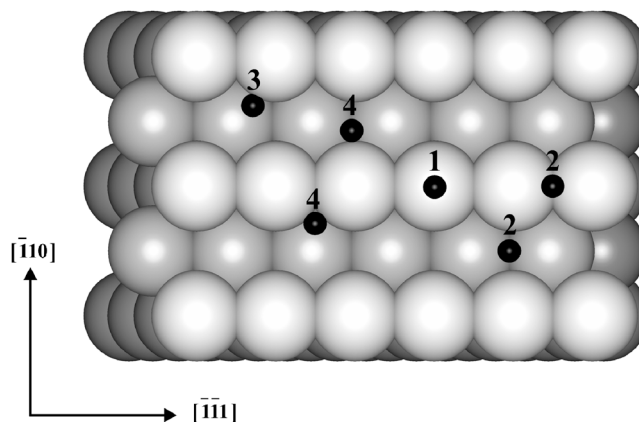


FIG. 1. Top view of the Mo(112) surface and the possible oxygen adsorption sites: (1) atop, (2) short-bridge, (3) long-bridge, and (4) pseudothreefold hollow. O atoms are shown as black spheres. For clarity, Mo atoms from the first layer are white, and the second and third layers are gray shaded.

ber of oxygen atoms are adsorbed in pseudothreefold hollow ( $O_2$ ) and short-bridge ( $O_1$  and  $O_3$ ) sites. Model A contains four oxygen atoms ( $n=4$ ) adsorbed in short-bridge sites on the first and third Mo rows ( $O_1$  and  $O_3$ ) and pseudothreefold hollow sites bound to one first layer Mo and two second layer Mo atoms ( $O_2$ ). In model B a single short-bridge oxygen ( $O_1$ ) is removed from the outermost Mo layer ( $n=3$ ). Model C contains two oxygen atoms ( $O_2$ ) per unit cell ( $n=2$ ) located in pseudothreefold hollow sites on both sides of the topmost Mo row. Models D and E have been suggested by Santra *et al.*<sup>9</sup> and Sasaki *et al.*,<sup>8</sup> respectively. The structure proposed by Santra *et al.*<sup>9</sup> (Fig. 2, model D) is similar to

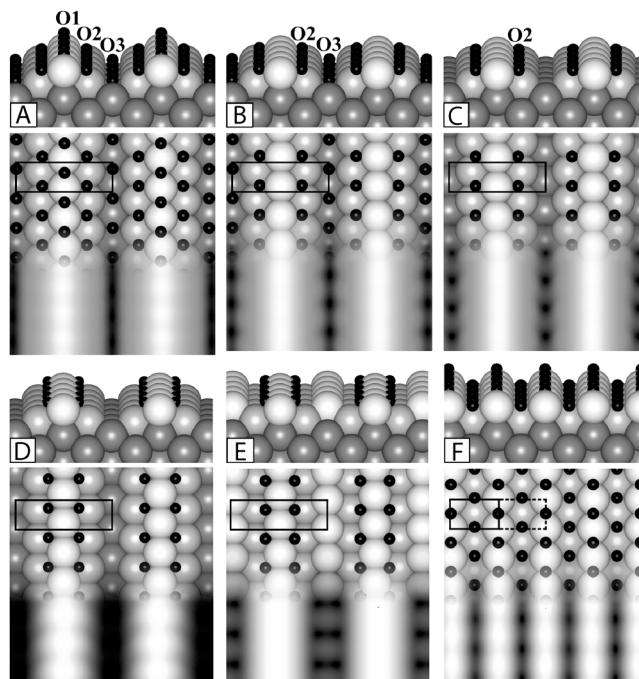


FIG. 2. Perspective and top views of the calculated  $p(1 \times 2)\text{-Mo}(112)/nO$  structure models along with their simulated STM images (lower panel). Models A, B, C, and D show missing-row reconstructed Mo(112) surface with  $n=4, 3, 2,$  and  $2,$  respectively. Models E ( $n=2$ ) and F ( $n=4$ ) involve unreconstructed surface. D is the model of Santra *et al.* (Ref. 9) and E is the model of Sasaki *et al.* (Ref. 8). The surface unit cells are indicated as black rectangles. See Fig. 1 for color coding.

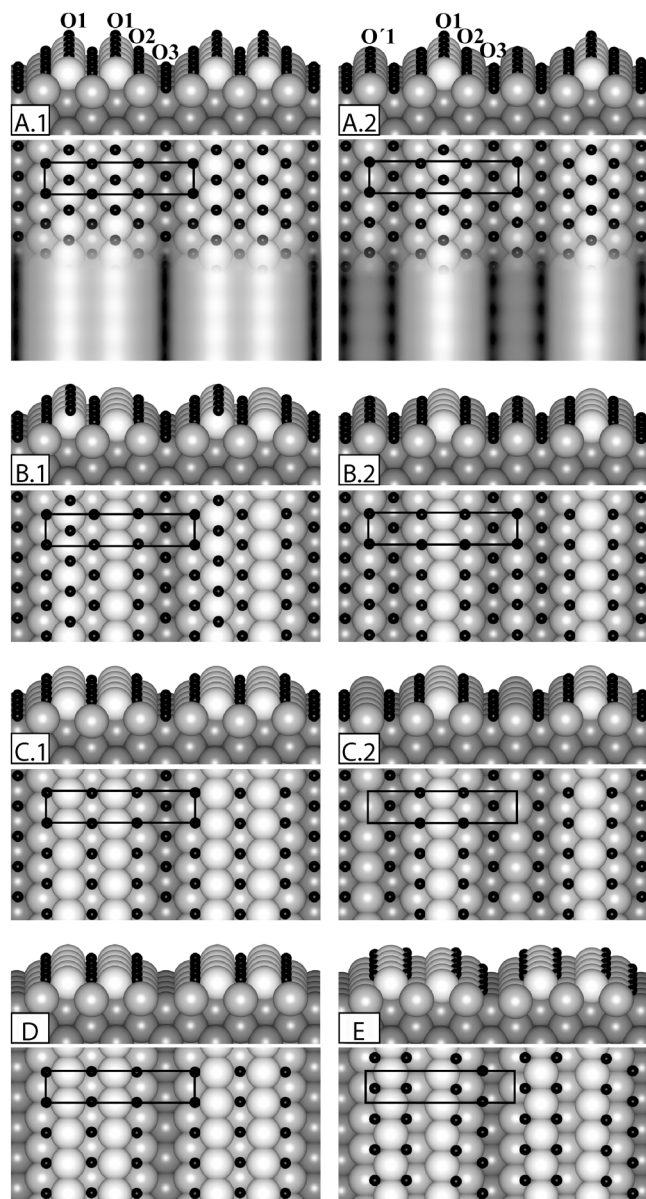


FIG. 3. Perspective and top views of the calculated  $p(1 \times 3)$ -Mo(112)/ $n$ O structure models along with simulated STM images (lower panel of A.1 and A.2). All models are characterized by missing-row reconstructed Mo(112) surfaces and varying amounts of oxygen atoms per unit cell;  $n=6$  (models A.1 and A.2),  $n=5$  (models B.1 and B.2),  $n=4$  (models C.1, C.2, and E), and  $n=3$  (model D). E is the model of Santra *et al.* (Ref. 9). The surface unit cells are indicated as black rectangles. See Fig. 1 for color coding.

model C but has a different bonding geometry of the oxygen atoms (two bonds to the first layer and one to the second layer Mo atoms,  $n=2$ ). It is also similar to the model suggested by Sasaki *et al.*<sup>8</sup> (Fig. 2, model E), which contains the same amount of oxygen atoms per surface unit cell ( $n=2$ ) in the same adsorption sites but involves a nonreconstructed Mo surface.

### B. $p(1 \times 3)$ -Mo(112)/ $n$ O models

The most stable  $p(1 \times 3)$ -Mo(112)/ $n$ O structure models obtained in our GA simulations are displayed in Fig. 3. Model E is identical to the structure proposed by Santra *et al.*<sup>9</sup> All models are characterized by a missing-row recon-

structed Mo(112) surface forming two reconstruction patterns. In the first pattern, denoted as the single missing-row reconstruction, every third row of Mo atoms along the  $[\bar{1}\bar{1}1]$  direction is missing (Fig. 3, models A.1, B.1, C.1, D, and E). In the second one, the double missing-row reconstruction, two missing rows are separated by one protruding Mo row (Fig. 3, models A.2, B.2, and C.2). Models A.1 and A.2 contain six O atoms ( $n=6$ ) located in the same adsorption sites as in the  $p(1 \times 2)$ -Mo(112)/4O structure (Fig. 2, model A), i.e., in short-bridge sites on the first and third Mo rows and in pseudothreefold hollow sites bound to one first layer Mo and two second layer Mo atoms. Additionally, model A.2 has O atoms adsorbed in short-bridge sites of the second Mo layer. In models B.1 and B.2 ( $n=5$ ) a single short-bridge oxygen atom is removed from the topmost Mo layer. In models C.1 and C.2 ( $n=4$ ) all short-bridge oxygen atoms from the first Mo layer (C.1) or first and second Mo layer (C.2) are removed. Further removal of O atoms bound to the third Mo layer results in model D ( $n=3$ ). The model of Santra *et al.*<sup>9</sup> (Fig. 3, model E) contains three oxygen atoms adsorbed in pseudothreefold hollow sites bound to two first layer Mo and one second layer Mo atoms, as well as one oxygen bound to two second layer Mo and one third layer Mo atoms ( $n=4$ ).

### C. Energies and stabilities

The calculated binding energies of oxygen atoms on the Mo(112) surface,  $\Delta E_b$ , vary between 2.8 and 3.7 eV. For the topmost short-bridge O atoms (O1) the predicted  $\Delta E_b$  values of 2.8–2.9 eV are similar for  $p(1 \times 2)$  and  $p(1 \times 3)$  models. Removal of the short-bridge oxygen atom located on the first Mo layer in the  $p(1 \times 3)$ -Mo(112)/5O model B.1 requires 3.2 eV. Approximately the same value is needed to remove the short-bridge oxygen atom from the second Mo layer (O'1, Fig. 3) in model B.2 (3.3 eV). The values of  $\Delta E_b$  for the short-bridge oxygen atoms located on the third Mo layer are about 3.6 eV in all models.

Figure 4 shows the surface-related free energy change of formation  $\Delta\gamma(T, p)$  of the most stable  $p(1 \times 2)$ -Mo(112)/ $n$ O and  $p(1 \times 3)$ -Mo(112)/ $n$ O structure models as a function of the oxygen chemical potential  $\Delta\mu_O$  and oxygen pressure at 1200 K. At high oxygen chemical potentials ( $\Delta\mu_O > -2.8$  eV) the most favorable structure is  $p(1 \times 2)$ -Mo(112)/4O (Fig. 2, model A). The  $p(1 \times 2)$ -Mo(112)/3O model (Fig. 2, model B) becomes stable at lower  $\Delta\mu_O$  values ( $-3.6 < \Delta\mu_O < -2.8$  eV). Finally, at very reducing conditions ( $\Delta\mu_O < -3.6$  eV), missing-row reconstructed structures with only two oxygen atoms per unit cell (Fig. 2, models C and D) are stabilized. Both models are almost equally stable ( $\Delta E_{\text{form}}$  differ by about 30 meV), which demonstrates that the precise bonding geometry of the oxygen atoms on the Mo(112) surface in pseudothreefold sites is difficult to determine. The two structures are more stable than the nonreconstructed model suggested by Sasaki *et al.*<sup>8</sup> (Fig. 2, model E). It should be stressed, that for the same surface unit composition the missing-row reconstructed structures are 0.36 eV ( $n=2$ ) to 0.56 eV ( $n=4$ ) more stable than the corresponding nonreconstructed ones.

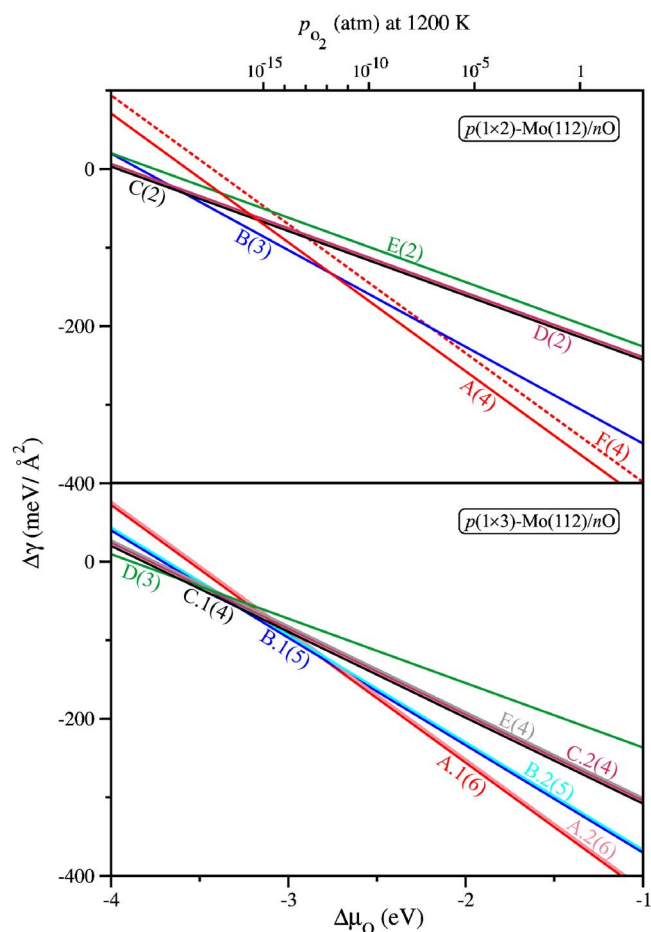


FIG. 4. (Color online) Surface-related free energy change of formation  $\Delta\gamma(T, p)$  for the most stable  $p(1 \times 2)$ -Mo(112)/ $n$ O (upper panel) and  $p(1 \times 3)$ -Mo(112)/ $n$ O (lower panel) structure models as a function of the oxygen chemical potential  $\Delta\mu_{\text{O}}$ . Numbers in parentheses indicate the amount of oxygen atoms ( $n$ ) per surface unit cell. In the top x axis the dependence on  $\Delta\mu_{\text{O}}$  has been cast into a pressure scale at 1200 K.

Very similar results are obtained for the  $p(1 \times 3)$ -Mo(112)/ $n$ O models. At high oxygen chemical potentials ( $\Delta\mu_{\text{O}} > -2.9$  eV) structures with a maximum oxygen occupancy ( $n=6$ ), i.e., A.1 and A.2 are the most stable. They are characterized by different reconstruction patterns (single versus double missing-row reconstruction). However, their formation energies differ by less than 0.15 eV only and the energy gain due to the reconstruction of the Mo(112) surface is 0.42 and 0.57 eV for models A.1 and A.2, respectively. At lower  $\Delta\mu_{\text{O}}$  values, structures with  $n=5$  (Fig. 3, models B.1 and B.2) and  $n=4$  (model C.1 and C.2) are energetically most favorable. The model proposed by Santra *et al.*<sup>9</sup> (Fig. 3, model E) which has the same amount of oxygen atoms per surface unit cell as models C.1 and C.2 is almost equally stable. Finally, at even further reducing conditions ( $\Delta\mu_{\text{O}} < -3.6$  eV) model D (Fig. 3) with  $n=3$  becomes most favorable.

Figure 5 compares the stability regions of the most stable  $p(1 \times 2)$ - and  $p(1 \times 3)$ -Mo(112)/ $n$ O models as a function of the oxygen chemical potential  $\Delta\mu_{\text{O}}$ . Our calculations demonstrate that in all cases oxygen adsorption on the Mo(112) surface induces missing-row-type reconstructions. Moreover, a coexistence of different  $p(1 \times 2)$  and  $p(1 \times 3)$

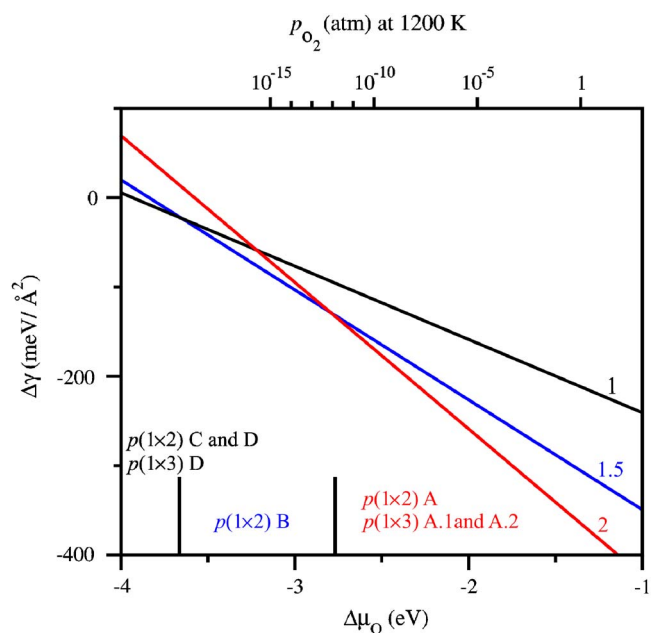


FIG. 5. (Color online) Stability regions of different  $p(1 \times 2)$ - and  $p(1 \times 3)$ -Mo(112)/ $n$ O structure models as a function of the oxygen chemical potential  $\Delta\mu_{\text{O}}$ . Numbers above the lines indicate the amount of oxygen atoms per  $(1 \times 1)$  Mo(112) unit cell.

structures is predicted. For  $\Delta\mu_{\text{O}} > -2.8$  eV structure models with the maximum oxygen occupancy (Fig. 2, model A and Fig. 3, models A.1 and A.2) become energetically most favorable. There is a range of oxygen chemical potential ( $-3.6$  eV  $< \Delta\mu_{\text{O}} < -2.8$  eV) for which only  $p(1 \times 2)$  model B is favored. At very reducing conditions the  $p(1 \times 2)$  models C and D as well as  $p(1 \times 3)$  model D, all containing exclusively pseudothreefold coordinated oxygen atoms on both sides of the Mo rows, are predicted to be the most stable.

## D. Experimental results

The chemisorption of oxygen on Mo(112) was studied experimentally using recipes reported in the literature for the preparation of various ordered structures. We focused on the formation of oxygen-induced  $p(1 \times 2)$  and  $p(1 \times 3)$  structures because of their relative simplicity compared to other structures formed at low oxygen coverages.

Formation of a pure  $p(1 \times 2)$  LEED pattern, shown in Fig. 6(b), was observed by dosing 6 L of  $\text{O}_2$  at 850 K, i.e., at pressure and temperature which fall in the range of the conditions reported for the preparation of ordered O/Mo(112) structures. The STM image of the  $p(1 \times 2)$  surface [Fig. 6(c)] shows extended rows with a periodicity of approximately 9.0 Å in the  $[\bar{1}10]$  direction, i.e., two times the spacing of Mo(112). The height difference between bright and dark stripes is approximately 1.0 Å.

Increasing the exposure of oxygen [30 L  $\text{O}_2$  was dosed at 300 K and then the sample was heated to 850 K for Fig. 6(d), while 40 and 50 L were used for Figs. 6(e) and 6(f), respectively] resulted in diffuse LEED patterns [see Figs. 6(d)–6(f)], which were interpreted as a combination of  $p(1 \times 2)$  and  $p(1 \times 3)$  phases. Attempts to form a pure  $p(1 \times 3)$

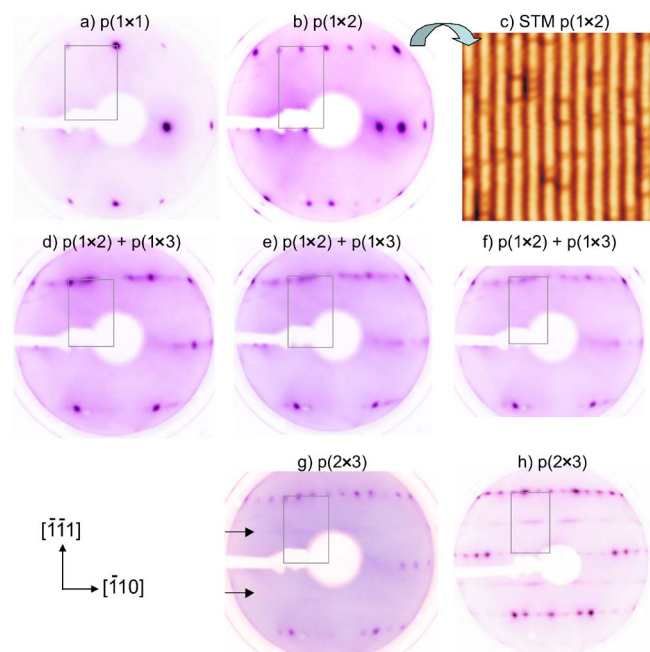


FIG. 6. (Color online) LEED patterns of oxygen-induced ordered structures on Mo(112). The  $(1 \times 1)$  pattern of the clean Mo(112) surface is shown in (a) and used as a reference for the other patterns. Figures (a) and (b) were collected at 72 eV. Figures (d)–(h) were collected at 100 eV. A high resolution STM image ( $10 \times 10 \text{ nm}^2$ ) of a  $p(1 \times 2)$ -Mo(112)/nO is shown on (c) (tunneling parameters:  $V_s = +2 \text{ V}$ ,  $I = 0.4 \text{ nA}$ ). The bright rows of oxygen separated by  $\sim 9.0 \text{ \AA}$  are clearly resolved. The crystallographic orientation indicated in the lower-left corner applies to all LEED and STM figures.

structure always resulted in the formation of a  $p(2 \times 3)$  phase shown in Fig. 6(g). Formation of streaks instead of spots, marked by the arrows in Fig. 6(g), indicates the presence of a high density of antiphase domain boundaries, as previously pointed out by Schroeder *et al.*<sup>11</sup> Following a recipe to produce the  $p(1 \times 3)$  surface reported in Ref. 9, the LEED pattern shown on Fig. 6(g) was obtained, which at first glance could be assigned to a pure  $p(1 \times 3)$  structure. However, close inspection of this pattern at different energies showed less intense but streaky spots corresponding to the initial formation of the  $p(2 \times 3)$  structure. A fully developed  $p(2 \times 3)$  structure, obtained following established procedures,<sup>11</sup> is shown as a reference in Fig. 6(h). Therefore, in agreement with our calculations, the LEED results show that the  $p(1 \times 3)$  structure is basically metastable under the conditions applied and often coexist with either  $p(1 \times 2)$  or  $p(2 \times 3)$  phases.

The XPS measurements of the O1s region for the  $p(1 \times 2)$  surface revealed an abnormally asymmetric peak with a maximum at 530.4 eV, as shown in Fig. 7. Attempts to fit the spectrum with a single component, using a convolution of a Gaussian and a Lorentzian contribution with a Doniach-Šunjić line shape, required an asymmetry parameter significantly above that normally used for single site oxygen adsorbate components on metals.<sup>27,28</sup> The high asymmetry clearly indicates the existence of at least two different O species. This finding is inconsistent with the  $p(1 \times 2)$  models C and D (the latter one suggested by Santra *et al.*<sup>9</sup>) as well as E (suggested by Sasaki *et al.*<sup>8</sup>), which both contain only one type of oxygen atoms. The only structures involving more

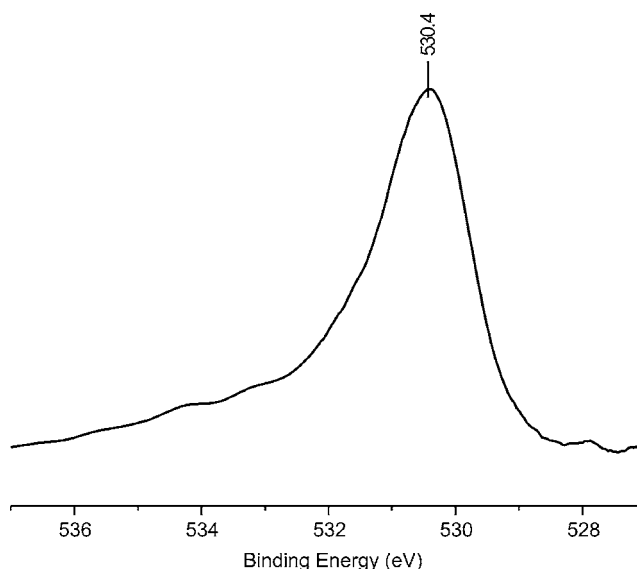


FIG. 7. O 1s region XPS of a  $p(1 \times 2)$ -Mo(112)/nO structure.

than one type of O atoms are the  $p(1 \times 2)$  models A, B, and F (Fig. 2). However, our calculations predict that the  $p(1 \times 2)$  model A coexists with  $p(1 \times 3)$  models A.1 and A.2. Therefore, we conclude that model B corresponds to the atomic structure of the observed pure  $p(1 \times 2)$  phase.

## E. Properties

Further verification of the structure models found in our generic algorithm simulations is obtained by comparison of the calculated and experimental STM images and vibrational spectra. Figure 2 shows the simulated STM images for the  $p(1 \times 2)$ -Mo(112)/nO models. The tip height is set to about  $4 \text{ \AA}$  above the highest atom and the simulation voltage is 1.5 V. Tunneling towards occupied or empty states, as well increasing the tip height up to  $5 \text{ \AA}$ , does not affect the simulated images. In a very good agreement with the experimental data [Fig. 6(c)] all structures show an alternation of bright and dark stripes. The protrusions are attributed to the first layer Mo atoms, whereas missing Mo rows are imaged as dark stripes. Simulations of the  $p(1 \times 2)$  models A–E give rise to similar images, indicating that STM cannot be used to distinguish between these structures. Only for the  $p(1 \times 2)$  model A oxygen atoms located on the topmost Mo rows (O1) seem to be imaged as brighter spots (Fig. 2, model A). Figure 3 shows the simulated STM images of the  $p(1 \times 3)$  models A.1 and A.2. The single and double missing-row reconstructed surface models have different ratios of bright and dark stripes (2:1 in the single A.1 and 1:2 in the double A.2 missing-row model). Similar to the  $p(1 \times 2)$  structures oxygen atoms located in the trenches (short-bridge sites on the third Mo layer) are not visible. For all models with the missing-row-type surface reconstruction the calculated corrugation is about  $1.0 \text{ \AA}$ , in agreement with our experimental data.

The experimental HREEL spectrum<sup>8</sup> of the  $p(1 \times 2)$ -Mo(112)/nO surface showed three main vibrational features at 220, 460, 620  $\text{cm}^{-1}$  and a shoulder at 670  $\text{cm}^{-1}$ .

TABLE I. Calculated scaled (scaling factor 1.0382) harmonic frequencies ( $\text{cm}^{-1}$ ) and their assignment for the most stable  $p(1 \times 2)$ -Mo(112)/ $n\text{O}$  structure models.

$p(1 \times 2)$ -A		$p(1 \times 2)$ -B		$p(1 \times 2)$ -C		$p(1 \times 2)$ -D	
$\nu^s(\text{Mo-O1/O2})$	717	$\nu^s(\text{Mo-O2})$	671	$\nu^s(\text{Mo-O2})$	632		614
$\nu^{as}(\text{Mo-O2})$	669	$\nu^{as}(\text{Mo-O2})$	651	$\nu^{as}(\text{Mo-O2})$	626		648
$\nu^{as}(\text{Mo-O1/O2})$	662						
$\nu^s(\text{Mo-O3})$	636	$\nu^s(\text{Mo-O3})$	611				
$\sigma(\text{Mo-O2})$	505	$\sigma(\text{Mo-O2})$	504	$\sigma(\text{Mo-O2})$	477		443
$\omega(\text{Mo-O2})$	481			$\omega(\text{Mo-O2})$	418		472
$\tau(\text{Mo-O2})$	471			$\tau(\text{Mo-O2})$	404		428
$\rho(\text{Mo-O2})$	457	$\rho(\text{Mo-O2})$	492	$\rho(\text{Mo-O2})$	456		448
$\delta_1^s(\text{Mo-O3/O1})$	456	$\delta_1^s(\text{Mo-O3})$	454				
$\delta(\text{Mo-O1/O2})$	434	$\delta(\text{Mo-O2})$	438/437				
$\delta_2^s(\text{Mo-O3/O1})$	299	$\delta_2^s(\text{Mo-O3})$	307				
$\delta_2^{as}(\text{Mo-O1/O3})$	276						

Oxygen exposure and annealing to 1000 K yields two additional peaks at 770 and 970  $\text{cm}^{-1}$ . The peak at 220  $\text{cm}^{-1}$  is typical for a clean Mo(112) surface and has been assigned to a dipole active surface resonance.<sup>29</sup> The modes at 460 and 620  $\text{cm}^{-1}$  were assigned to pseudothreefold coordinated oxygen atoms. The 670  $\text{cm}^{-1}$  mode was assigned to molecularly adsorbed oxygen and in particular to bridged peroxo species, and the 770  $\text{cm}^{-1}$  mode which appears after annealing to 1000 K was associated with the loss of surface order and formation of three-dimensional  $\text{Mo}_x\text{O}_y$  phases.<sup>8</sup> A similar vibration at 725  $\text{cm}^{-1}$  has been attributed to the surface oxide  $\text{MoO}_2$  formed after oxygen adsorption on the Mo(111) surface.<sup>32</sup>

Table I summarizes the frequencies and vibrational modes of oxygen-related vibrations calculated for the  $p(1 \times 2)$  models A–D. Graphical representations of the normal modes are shown in Fig. 8. Both  $p(1 \times 2)$  and  $p(1 \times 3)$ -Mo(112)/ $n\text{O}$  structure models found in our calculations have similar oxygen adsorption sites and show very similar vibrational spectra. Therefore, we restrict the discussion of the vibrational modes to  $p(1 \times 2)$ -Mo(112)/ $n\text{O}$  structures only. For all models the calculated frequencies fall into the range of observed HREELS vibrations. In the model B

(Fig. 2), which is the most stable structure for the pure  $p(1 \times 2)$  phase, the calculated vibrational frequencies at 671 and 651  $\text{cm}^{-1}$  are assigned to symmetric and asymmetric stretching modes, respectively [ $\nu^s(\text{Mo-O2})$  and  $\nu^{as}(\text{Mo-O2})$ , Figs. 8(a) and 8(b)] of the threefold coordinated oxygen atoms (O2). The stretching mode of the short-bridge oxygen atoms [ $\nu^s(\text{Mo-O3})$ , Fig. 8(d)] is located at 611  $\text{cm}^{-1}$ . In addition, vibrational spectrum of the model B shows deformation modes for the adsorbed oxygen species, scissoring [Fig. 8(e)] at 504  $\text{cm}^{-1}$ , rocking [Fig. 8(h)] at 492  $\text{cm}^{-1}$ , as well as deformation modes involving movements of short-bridge oxygen atoms [Figs. 8(i)–8(k)] at 307–454  $\text{cm}^{-1}$ . Vibrational spectra of models C and D are similar but additionally involve wagging modes [Fig. 8(f)] at 418 and 472  $\text{cm}^{-1}$ , as well as twisting deformation modes [Fig. 8(g)] at 404 and 428  $\text{cm}^{-1}$ , respectively. Further oxidation of the  $p(1 \times 2)$  model B leads to adsorption of additional oxygen atoms in the short-bridge sites on the topmost Mo layer (O1, Fig. 2), resulting in the  $p(1 \times 2)$  model A. For this model the highest vibrational frequency at 717  $\text{cm}^{-1}$  is associated with a symmetric coupled stretching of the O1 and O2 atoms on the Mo(112) surface [Fig. 8(a)]. The asymmetric

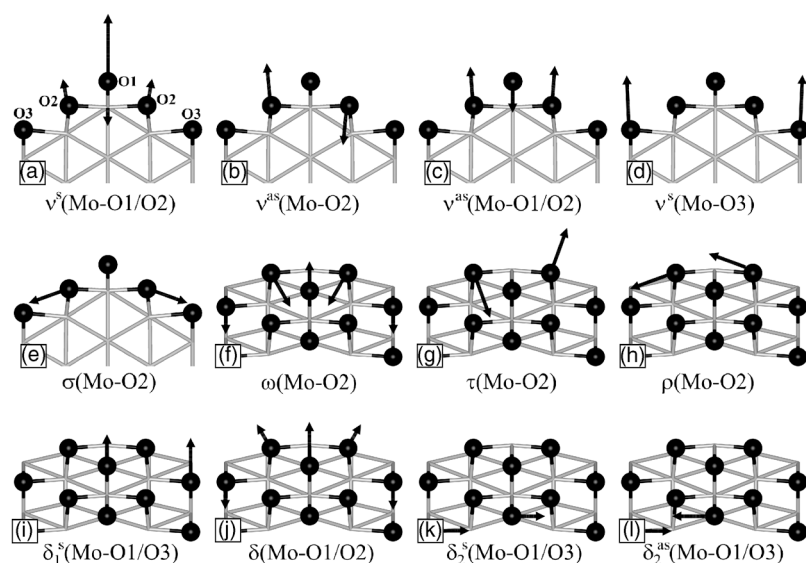


FIG. 8. Calculated vibrational normal modes for the  $p(1 \times 2)$  model A. Side view images (a)–(d) show the stretching modes, whereas the side view image (e) is the scissoring mode. (f)–(l) are top views of different deformation modes. The oxygen atoms are drawn as black balls and the Mo(112) surface is shown as gray sticks.

mode of this vibration [Fig. 8(c)] located at  $662\text{ cm}^{-1}$  is very similar to the asymmetric stretching mode involving O2 atoms only. At the same time, the pure stretching vibration of the O3 oxygen atoms [ $\nu^s(\text{Mo-O3})$ , Fig. 8(d)] is shifted by about  $25\text{ cm}^{-1}$  towards higher frequencies as compared to the same mode in the  $p(1\times 2)$  model B. The frequencies of deformation vibrations for model A vary between  $276$  and  $505\text{ cm}^{-1}$ , with the lowest frequency mode assigned to the asymmetric translation of O1 and O3 atoms [Fig. 8(l)].

Finally, we note, that infrared reflection absorption spectroscopy (IRAS) experiments on the oxygen-induced  $p(2\times 3)$ -Mo(112) structure reveal an intense vibrational mode at  $990\text{ cm}^{-1}$ .<sup>30</sup> This vibration has been assigned to the stretching mode of oxygen atoms adsorbed on top of Mo atoms, thus forming Mo=O double bond, exhibiting a characteristic band in the range of  $980$ – $1010\text{ cm}^{-1}$ .<sup>30–33</sup> Although no stable structure containing double Mo=O bonds was found in our simulations, we can indirectly confirm this assignment. The highest vibrational frequency involving single Mo–O bonds is at  $717\text{ cm}^{-1}$ , indicating that the vibration observed at  $990\text{ cm}^{-1}$  must involve bonds of higher orders.

## V. SUMMARY AND CONCLUSIONS

We have demonstrated the power of the genetic algorithm combined with density functional theory for predicting the atomic surface structures formed upon adsorption of oxygen on the Mo(112) substrate. Our simulations of  $p(1\times 2)$  and  $p(1\times 3)$  structures point to an unusual flexibility of the Mo(112) surface which easily undergoes missing-row-type reconstruction. The  $p(1\times 2)$  and  $p(1\times 3)$  structural models found here are more stable than any other model suggested so far and involve only two oxygen adsorption sites, i.e., short-bridge and pseudothreefold hollow sites. Comparison of the stabilities of the predicted models shows that different  $p(1\times 2)$  and  $p(1\times 3)$  structures may coexist over a wide range of oxygen pressures. A pure  $p(1\times 2)$  structure can be obtained only in a narrow region of oxygen pressures. In contrast, a pure  $p(1\times 3)$  structure cannot exist as a stable phase. These findings are fully supported by our LEED results. Combining theoretical predictions and experimental STM and XPS data allows for an unequivocal determination of the atomic model of the observed  $p(1\times 2)$  structure. It contains three O atoms per unit cell and involves a missing-row-type reconstruction (Fig. 2, model B). Finally, we provide an assignment of the vibrational modes observed in HREELS experiments for the  $p(1\times 2)$ -Mo(112)/ $n\text{O}$  surfaces.

## ACKNOWLEDGMENTS

The authors gratefully acknowledge financial support by Deutsche Forschungsgemeinschaft (DFG) and the Fonds der Chemischen Industrie. T.K.T. and S.K. acknowledge the International Max Planck Research School “Complex Surfaces in Materials Science” for fellowships. Two of the authors (D.S. and J.W.) thank the Alexander von Humboldt Foundation. The calculations were carried out at the Norddeutscher Verbund für Hoch- und Höchstleistungsrechnen (HLRN).

- <sup>1</sup>J. Haber, in *Molybdenum Compounds in Heterogeneous Catalysis*, Studies in Inorganic Chemistry Vol. 19, edited by E. R. Braithwaite and J. Haber (Elsevier, New York, 1994).
- <sup>2</sup>M. S. Chen, A. K. Santra, and D. W. Goodman, *Phys. Rev. B* **69**, 155404 (2004).
- <sup>3</sup>T. Schroeder, M. Adelt, B. Richter, M. Naschitzki, M. Bäumer, and H.-J. Freund, *Surf. Rev. Lett.* **7**, 7 (2000).
- <sup>4</sup>M.-C. Wu and D. W. Goodman, *J. Phys. Chem.* **98**, 9874 (1994).
- <sup>5</sup>M. S. Chen, W. T. Wallace, D. Kumar, Z. Yan, K. K. Gath, Y. Cai, Y. Kuroda, and D. W. Goodman, *Surf. Sci.* **581**, L115 (2005).
- <sup>6</sup>M.-C. Wu, J. S. Corneille, C. A. Estrada, J.-W. He, and D. W. Goodman, *Chem. Phys. Lett.* **182**, 472 (1991).
- <sup>7</sup>T. McAvoy, J. Zhang, C. Waldfried, D. N. McIlroy, P. A. Dowben, O. Zeybek, T. Bertrams, and S. D. Barrett, *Eur. Phys. J. B* **14**, 747 (2000).
- <sup>8</sup>T. Sasaki, Y. Goto, R. Tero, K. Fukui, and Y. Iwasawa, *Surf. Sci.* **502**, 136 (2002).
- <sup>9</sup>A. K. Santra, B. K. Min, and D. W. Goodman, *Surf. Sci.* **513**, L441 (2002).
- <sup>10</sup>K. Fukui, T. Aruga, and Y. Iwasawa, *Surf. Sci.* **281**, 241 (1993).
- <sup>11</sup>T. Schroeder, J. B. Giorgi, A. Hammoudeh, N. Magg, M. Bäumer, and H.-J. Freund, *Phys. Rev. B* **65**, 115411 (2002).
- <sup>12</sup>A. Kiejna and R. M. Nieminen, *J. Chem. Phys.* **122**, 044712 (2005).
- <sup>13</sup>F. C. Chuang, C. V. Ciobanu, V. B. Shenoy, C. Z. Wang, and K. M. Ho, *Surf. Sci.* **573**, L375 (2004).
- <sup>14</sup>F. C. Chuang, C. V. Ciobanu, C. Predescu, C. Z. Wang, and K. M. Ho, *Surf. Sci.* **578**, 183 (2005).
- <sup>15</sup>C. V. Ciobanu and C. Predescu, *Phys. Rev. B* **70**, 085321 (2004).
- <sup>16</sup>G. Kresse and J. Furthmüller, *Comput. Mater. Sci.* **6**, 15 (1996).
- <sup>17</sup>G. Kresse and J. Furthmüller, *Phys. Rev. B* **54**, 11169 (1996).
- <sup>18</sup>J. P. Perdew, J. A. Chevary, S. H. Vosko, K. A. Jackson, M. R. Pederson, D. J. Singh, and C. Fiolhais, *Phys. Rev. B* **46**, 6671 (1992).
- <sup>19</sup>P. E. Blöchl, *Phys. Rev. B* **50**, 17953 (1994).
- <sup>20</sup>G. Kresse and D. Joubert, *Phys. Rev. B* **59**, 1758 (1999).
- <sup>21</sup>H. J. Monkhorst and J. D. Pack, *Phys. Rev. B* **13**, 5188 (1976).
- <sup>22</sup>J. Tersoff and D. R. Hamann, *Phys. Rev. B* **31**, 805 (1985).
- <sup>23</sup>J. F. Scott and S. P. S. Porto, *Phys. Rev.* **161**, 903 (1967).
- <sup>24</sup>R. Srivastava and L. L. Chase, *Solid State Commun.* **11**, 349 (1972).
- <sup>25</sup>K. Reuter and M. Scheffler, *Phys. Rev. B* **65**, 035406 (2002).
- <sup>26</sup>D. E. Goldberg, *Genetic Algorithms in Search, Optimization & Machine Learning* (Addison-Wesley, Boston, 2005).
- <sup>27</sup>C. Puglia, A. Nilsson, B. Hernäs, O. Karis, P. Bennich, and N. Mårtensson, *Surf. Sci.* **342**, 1119 (1995).
- <sup>28</sup>J. Weissenrieder, M. Göthelid, M. Månsson, H. von Schenck, O. Tjernberg, and U. O. Karlsson, *Surf. Sci.* **527**, 163 (2003).
- <sup>29</sup>J. Kröger, S. Lehwald, and H. Ibach, *Phys. Rev. B* **55**, 10895 (1997).
- <sup>30</sup>T. Schroeder, Ph.D. thesis, Humboldt-Universität zu Berlin, 2002.
- <sup>31</sup>M. L. Colaizzi, J. G. Chen, W. H. Weinberg, and J. T. Yates, *Surf. Sci.* **279**, 211 (1992).
- <sup>32</sup>P. K. Stefanov and T. S. Marinova, *Surf. Sci.* **200**, 26 (1988).
- <sup>33</sup>K. T. Queeney and C. M. Friend, *J. Phys. Chem. B* **102**, 5178 (1998).